Proceedings of The Institute of Acoustics

SOUND INTENSITY DISTRIBUTIONS IN DUCTS

F.J. Fahy

Institute of Sound and Vibration Research, The University,
Southampton, SO9 5NH.

1. INTRODUCTION

The distribution of axial sound intensity in ducts, and its relationship to the associated mean square pressure distribution, is of practical concern in at least two areas of engineering acoustics. For many years work has been proceeding on the development of standards for the in-duct determination of the sound power generated by air-moving devices. Progress has been inhibited by the uncertainty of the relationship between the measurable quantity, namely mean square pressure, and the quantity required, namely axial sound intensity. The other problem to which this question is relevant is that of the estimation of pipe wall vibration by sound in the contained fluid, and the consequent radiation of sound power; this is the pipe wall transmission problem. The most readily estimated input quantity is the sound power injected into a pipe by sound generating mechanisms such as flow through valves; the agent which creates pipe wall vibration is the fluctuating wall pressure; the relationship between the two is currently subject to considerable uncertainty. The investigation of this relationship presented here is only at an early stage, but it is hoped that the results will illustrate the potential usefulness of sound intensity measurements in duct acoustic problems.

2. THEORETICAL CONSIDERATIONS

A linear acoustic field in a uniform section of duct which carries ideal, non-turbulent, mean flow, may be represented as the superposition of the characteristic spatial functions, or acoustic modes, of the duct: these are determined by the duct cross section geometry together with the wall boundary conditions. The acoustic pressure and axial particle velocity at a point in a duct may each be represented by the same modes; they are linked by the fluid momentum equation in the axial direction, which is a function of the local Mach number of the mean flow in the duct. If the mean velocity vector is non-uniform over a cross section, and also, possibly, not directed purely axially, the resulting problem of solving for the duct modes and their propagation characteristics, is rather complex. In the following analyses, we shall assume that mean flow is absent (M = 0), in order to clarify the issue of the pressure-intensity relationship.

Consider a two-dimensional uniform duct of width a with rigid walls. The harmonic modal pressure distributions take the form

$$p_m(x,y,t) = \cos(m\pi y/a)\left[\tilde{A}_m \exp(-ik_m x) + \tilde{B}_m \exp(ik_m x)\right] e^{i\omega t}, \qquad (1)$$

in which a is the duct width, and the axial wavenumber component

$$k_m = \left[k^2 - (m\pi/a)^2\right]^{\frac{1}{2}};$$

SOUND INTENSITY DISTRIBUTIONS IN DUCTS

positive-going waves have complex amplitude $\tilde{A}_m$ and negative-going waves have complex amplitude $\tilde{B}_m$. At frequencies for which $k > m\pi/a$, or $f > mc/2a$ (Hz) the mode may propagate freely up and down the length of the duct. If $f < mc/2a$, the mode may not propagate, but is evanescent, and decays exponentially with axial distance from the point of its generation (by a source, or by scattering out of other modes at a discontinuity). The frequency $f_m = mc/2a$ is the mode cut-off frequency. In zero mean flow, the corresponding axial particle velocity has the distribution

$$u_m(x,y,t) = (k_m/\omega\rho_o)\cos(m\pi y/a)\left[\tilde{A}_m\exp(-ik_m x) - \tilde{B}_m\exp(ik_m x)\right]e^{i\omega t} \qquad (2a)$$

at frequencies above f_m, and

$$u_m(x,y,t) = (ik'_m/\omega\rho_o)\cos(m\pi y/a)\left[-\tilde{A}_m\exp(-k'_m x) + \tilde{B}_m\exp(k'_m x)\right]e^{i\omega t} \qquad (2b)$$

at frequencies below f_m, where $k'_m = \left[(m\pi/a)^2 - k^2\right]^{\frac{1}{2}}$.

For simplicity we now neglect negative-going waves ($\tilde{B}_m = 0$), and consider the mean axial sound intensity in a field which is represented by the superposition of modes: the total field pressure is:

$$p(x,y,t) = \Big\{\sum_{m=m_1}^{\infty}\cos(m\pi y/a)\left[\tilde{A}_m\exp(-ik_m x)\right] + \sum_{m=0}^{m_1-1}\cos(m\pi y/a)\left[\tilde{A}_m\exp(-k'_m x)\right]\Big\}e^{i\omega t}, \qquad (3)$$

and the total field particle velocity is

$$u(x,y,t) = \Big\{\sum_{m=m_1}^{\infty}(k_m/\omega\rho_o)\cos(m\pi y/a)\left[\tilde{A}_m\exp(-ik_m x)\right] - \sum_{m=0}^{m_1-1}(ik'_m/\omega\rho_o)\cos(m\pi y/a) \times \left[\tilde{A}_m\exp(-k'_m x)\right]\Big\}e^{i\omega t}, \qquad (4)$$

in which propagating and evanescent modes have been separated. The mean axial intensity is given by

$$\bar{I}_x(x,y) = \tfrac{1}{2}\,\mathrm{Re}\{\tilde{P}(x,y)\tilde{U}^*(x,y)\}, \qquad (5)$$

where $p(x,y,t) = \tilde{P}(x,y)e^{i\omega t}$ and $u(x,y,t) = \tilde{U}\,e^{i\omega t}$, $\tilde{P}$ and $\tilde{U}$ being given by equations (4) and (5). Four sets of products appear, two of them involving products of propagating and evanescent modes: the intensity distribution is clearly rather complicated, especially near sources or other generators of significant evanescent modal disturbances. However, if an expression is formed for the total sound power passing through any cross section, the orthogonal property of the modes, together with the quadrature relationship of pressure to velocity in evanescent modes, ensures that only the sum of the powers transmitted by each propagating mode in isolation remains.

SOUND INTENSITY DISTRIBUTIONS IN DUCTS

In order to simplify the picture let us confine our attention to the two lowest order modes, namely m = 0 (plane wave) and m = 1. Consider a frequency below $f_1 = c/2a$: mode 0 propagates but mode 1 is evanescent. Equation (5) becomes

$$\bar{I}_x(x,y) = \tfrac{1}{4}\,\mathrm{Re}\{\left[\tilde{A}_0\exp(-ikx) + \cos(\pi y/a)\tilde{A}_1\exp(-k_1'x)\right] \times \left[(1/\rho_o c)\tilde{A}_0^{*}\exp(ikx) + (ik_1'/\omega\rho_o)(\cos\pi y/a)\tilde{A}_1^{*}\exp(-k_1'x)\right]\}. \quad (6)$$

The four contributions to axial intensity are as follows:

$$\bar{I}_{00} = |\tilde{A}_0|^2/2\rho_o c; \qquad \bar{I}_{11} = 0;$$

$$\bar{I}_{01} = (k_1'/2\omega\rho_o)\cos(\pi y/a)\exp(-k_1'x)\left[(A_{0r}\cos kx + A_{0i}\sin kx)(A_{1i}) - (A_{0i}\cos kx - A_{0r}\sin kx)(A_{1r})\right];$$

$$\bar{I}_{10} = (1/2\rho_o c)\cos(\pi y/a)\exp(-k_1'x)\left[(A_{0r}\cos kx + A_{0i}\sin kx)(A_{1r}) + (A_{0i}\cos kx - A_{0r}\sin kx)(A_{1i})\right], \quad (7)$$

where $\tilde{A}_0 = A_{0r} + iA_{0i}$ and $\tilde{A}_1 = A_{1r} + iA_{1i}$. $\bar{I}_x$ can therefore be positive at some values of x and y and negative at others. In addition to the axial intensity, there will be transversely directed components $I_y(x,y)$, so that circulation of intensity will occur. In the general case, "interaction" between propagating modes may also cause intensity circulation.

3. NUMERICAL STUDIES

In view of the extreme complexity of such fields, which precludes all except statistical analysis in the case of many propagating modes, distributions of intensity and mean square pressure in this simple model of a duct have been studied numerically on a microcomputer. Two methods are open: in one, the pressure and particle velocity fields are expressed by modal superposition; in the other, source image techniques may be used to form the rigid boundaries. The former approach has the advantage that the wall boundary conditions are satisfied, however severely the model series is truncated, but it has the disadvantage that the field near a source is not necessarily well represented; however, the appropriate truncation far from a source is known from the cut-off frequency. The latter approach has exactly the opposite properties to the former, the field representation by a limited array of images deteriorating with distance from the source: however, numerical problems at cut-off seem to be avoided. The latter method was chosen because a general source/intensity field program was already available, and high accuracy was not sought. It transpired from initial computations that an image order of ten gave acceptable accuracy for the range of parameters used.

Of particular interest was the comparison between band limited and single frequency excitation. For this purpose, the results of calculations of intensity and mean square pressure at single frequencies can be superimposed because pressure and particle velocities of different frequency cannot combine

to produce intensity in a linear system. Some examples of single and multiple frequency intensity distributions generated by a point monopole are shown in Figs. 1 and 2. The duct width 'a' is assumed to be 1 m (f_m = 171.5 m Hz). Figs. 1(a-c) show the influence of the first higher order mode ($\cos\pi y/a$) just below, and just above cut-off; note its absence with a central source. Figs. 2(a-f) show fields at frequencies much higher than the lowest cut-off frequency; the effect of multiple frequency excitation on "straightening out" and "filling in the gaps" in the axial intensity distribution is clearly seen in Figs. 2(b),(d) and (f). As expected, strong circulation only seems evident for single frequency excitation very near cut-off frequencies.

4. EXPERIMENTAL INVESTIGATION

As a complement to the theoretical analyses, an experimental investigation was conducted to measure the distributions of axial sound intensity and mean square pressure in a section of rigid duct of circular cross section: the internal diameter was 305 mm and the length was 2.7 m. A small loudspeaker of 140 mm diameter was placed at one opened end, and an intensity probe consisting of two phase matched, ½-inch, side-by-side microphones, separated by 15 mm, was introduced through the other open end. Measurements were made at a distance of 420 mm from this end, with the loudspeaker facing down the duct with its centre on the duct axis, and also with it 85 mm off axis: the measurement cross section was divided into 33 segments. Using a computer controlled, dual channel signal analyser, pressure auto spectra, together with the real part of the cross spectra between one microphone signal and the second integrated microphone signal, were output to the computer. The spectra were computed with a resolution of 10 Hz within the 100-5000 Hz measurement range; for ease of presentation these spectra were combined into 49 bands of 100 Hz width. The auto spectra and cross spectra, measured with the microphones aligned parallel to the duct axis, were compared by factoring the pressure spectra by a factor of $c/\Delta x$, where Δx was the microphone separation distance of 15 mm: in this way axial intensity was compared directly with $\overline{p^2}/\rho_o c$. A plane-wave finite separation correction was applied to the computed intensity values (e.g. 1.4 at 5 kHz). In addition to measurements made with a completely open end to the duct, a small number of tests were conducted with the end partially blocked by a rigid sheet which closed off three-quarters of the duct, leaving a cheese-shaped opening on one side.

Comparisons have been made between the spatial average value of $\overline{p^2}/\rho_o c$, and average value of $\overline{p^2}/\rho_o c$ close to the wall, and the spatial average axial intensity: these are plotted in Fig. 3. From this figure, and the corresponding samples of 10 Hz resolved spectra shown in Figs. 4(a) and 4(b), it is observed that there is remarkably little difference between these quantities, except at frequencies below the lowest cut-off frequency of the duct (660 Hz), where the duct end-reflection produces an axial interference field; the periodicity of the low frequency spectra (60 Hz) corresponds to integer numbers of half-wavelengths in the duct length. Indeed, except very close to some cut-off frequencies, the local auto and cross spectra were normally within 1 or 2 dB of each other at each point in the field. At the measurement distance used, negative intensity components were very rarely observed. This was not so when the partially blocked duct was tested; Fig. 5 shows that the scaled auto spectrum rises significantly above the cross spectrum, although the frequency average power levels did not fall by more than 1 or 2 dB: axial

interference is now seen to extend over the whole spectrum. Examples of linear intensity and $\overline{p^2}$ spectra shown in Fig. 6 illustrate the creation of local negative intensity regions by the end-reflection, and the rise in $\overline{p^2}$.

5. CONCLUSIONS

The following conclusions may tentatively be drawn from the results of these initial tests.

1. Despite the complicated form of the theoretical intensity vector distribution in a duct at frequencies well above its lowest cut-off frequency, measurements in an open-ended duct show that, above the lowest cut-off frequency, the axial intensity component, and the local value of $\overline{p^2}/\rho_o c$, follow each other remarkably closely (within 1-2 dB) at all points on a duct cross section quite far from the source, except in very narrow bands of frequency very close to some higher order mode cut-off frequencies. Hence the spatial average value of $\overline{p^2}/\rho_o c$ is very close to the spatial average intensity, except below the lowest cut-off frequency.

2. The effect of a significant end reflection is to introduce negative axial intensities into the duct and generally to raise local values of $\overline{p^2}/\rho_o c$ at individual points by 3-5 dB above the local axial intensity component; the in-duct power generated by a loudspeaker was not greatly changed by the end condition.

3. In practice, provided that a significant end reflection is not present, the in-duct sound power can be estimated rather accurately from mean square pressure measurement, even with many higher order modes present.

4. In the absence of significant end reflection, the average mean square wall pressure is given rather closely by $\overline{p^2} \approx \rho_o cW/S$, where in-duct sound power W passes through area S.

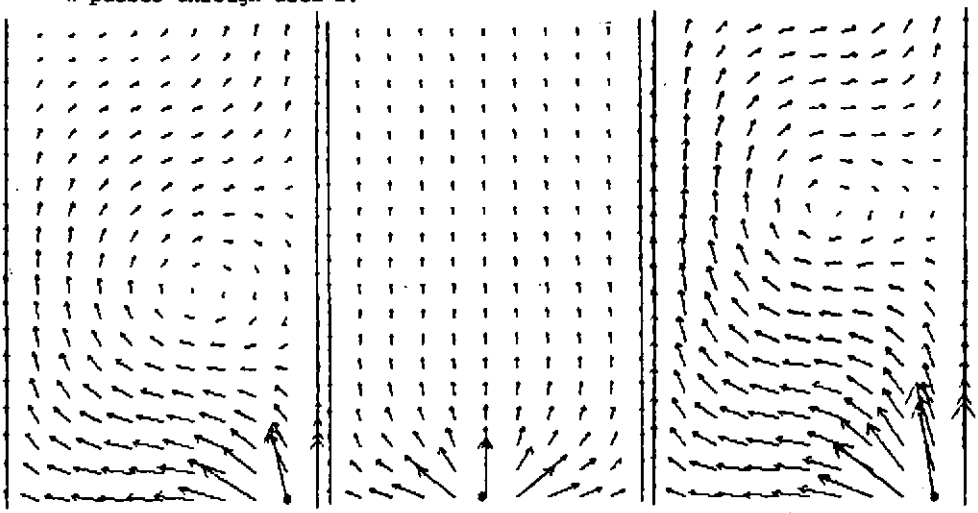

Fig. 1(a). 165 Hz. Fig. 1(b). 165 Hz. Fig. 1(c). 175 Hz.

SOUND INTENSITY DISTRIBUTIONS IN DUCTS

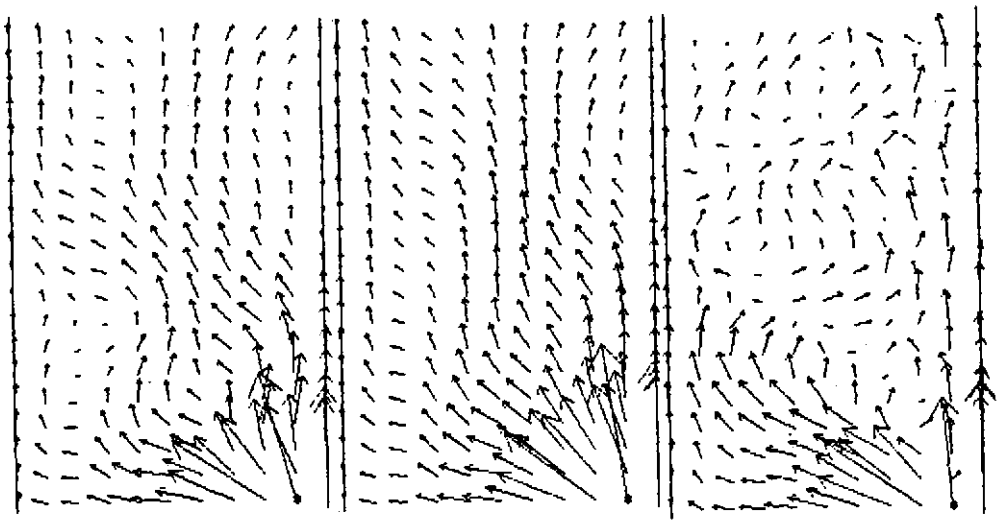

Fig. 2(a). 500 Hz.

Fig. 2(b). 450-550 Hz in 25 Hz steps.

Fig. 2(c). 2000 Hz.

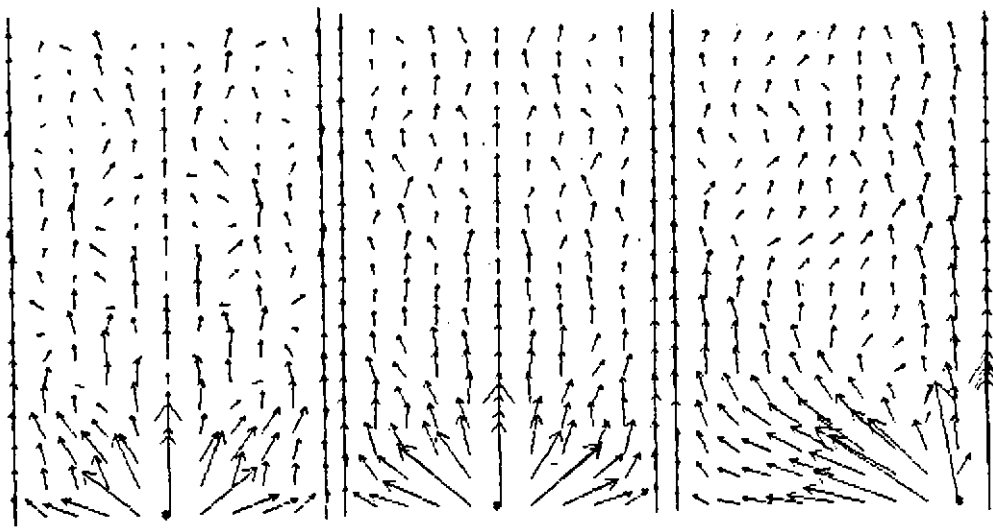

Fig. 2(e). 2000 Hz

Fig. 2(f). 1800-2200 Hz in 100 Hz steps.

Fig. 2(d). 1800-2200 Hz in 100 Hz steps.

SOUND INTENSITY DISTRIBUTIONS IN DUCTS

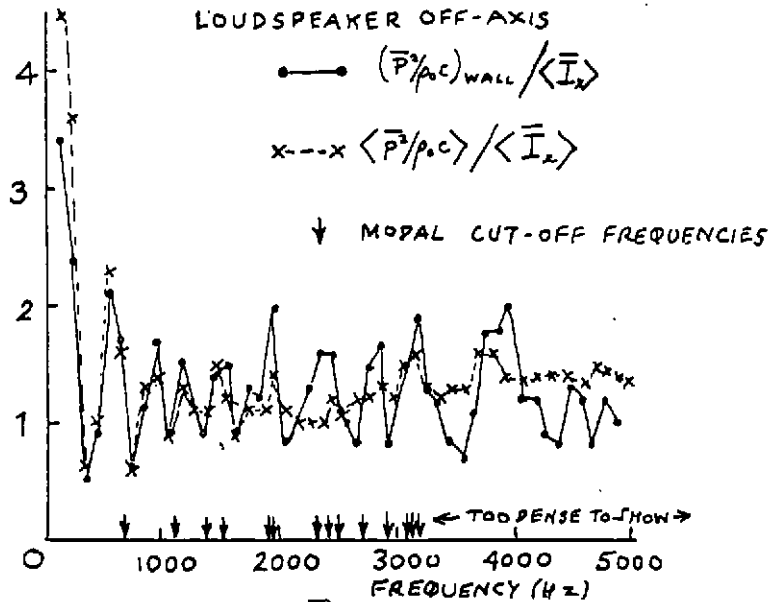

Fig. 3. Ratio of average $\overline{p}^2/\rho_o c$ to average axial intensity in the open-ended duct.

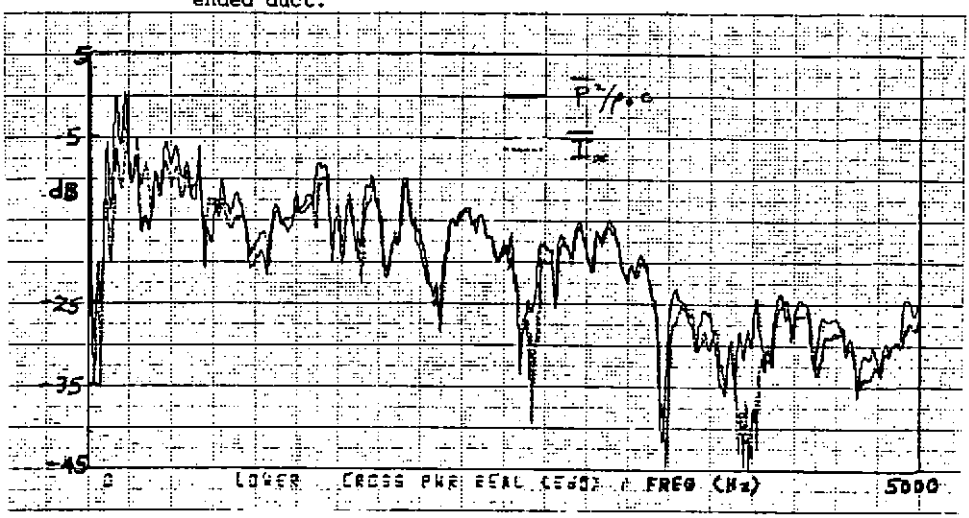

Fig. 4(a). Spectra of $\overline{p}^2/\rho_o c$ and axial intensity near to the wall in the open-ended duct.

SOUND INTENSITY DISTRIBUTIONS IN DUCTS

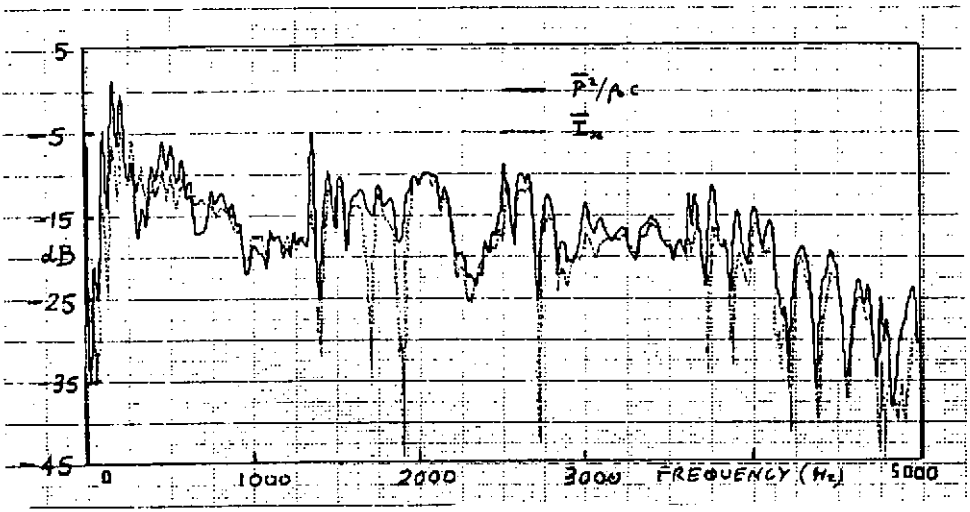

Fig. 4(b). Spectra of $\overline{p^2}/\rho_0 c$ and axial intensity on the axis of the open ended duct.

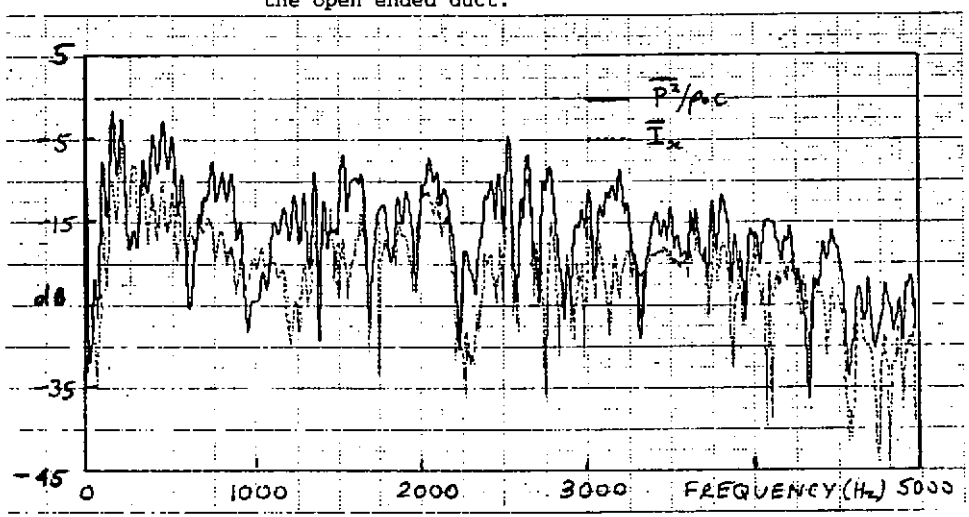

Fig. 5. Same position as Fig. 4(b) but with partially blocked duct opening.

SOUND INTENSITY DISTRIBUTIONS IN DUCTS

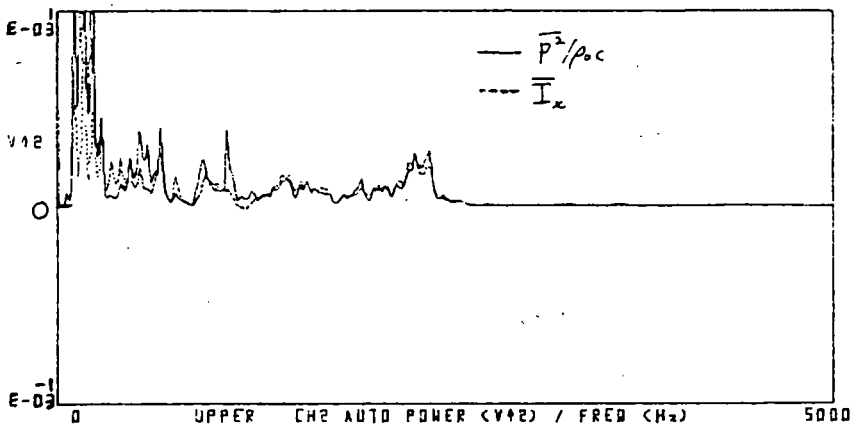

Fig. 6(a). Linear $\overline{p^2}/\rho_0 c$ and axial intensity spectra in the open ended duct.

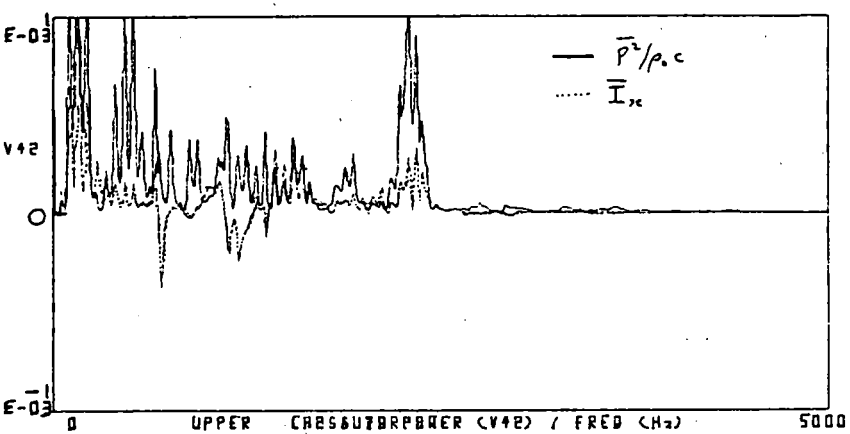

Fig. 6(b). As Fig. 6(a) but with a partially blocked end to the duct.